Journal of Marine Science and Technology

Volume 24 | Issue 3 Article 8

THE HYDRODYNAMIC CHARACTERISTICS OF AN INCLINED SUBMERGED POROUS PLATE WITH ROCK FILLED STRUCTURE

Ching-Yun Yueh
Department of Harbor and River Engineering, National Taiwan Ocean University Keelung, Taiwan, R.O.C.,
yuehcy@mail.ntou.edu.tw

Shih-Hsuan Chuang
Wayteng Technology Co., Ltd, Kaohsiung, Taiwan, R.O.C

Chih-Hao Su
Department of Harbor and River Engineering, National Taiwan Ocean University Keelung, Taiwan, R.O.C

Recommended Citation

Yueh, Ching-Yun; Chuang, Shih-Hsuan; and Su, Chih-Hao (2016) "THE HYDRODYNAMIC CHARACTERISTICS OF AN INCLINED SUBMERGED POROUS PLATE WITH ROCK FILLED STRUCTURE," *Journal of Marine Science and Technology*: Vol. 24: Iss. 3, Article 8.
DOI: 10.6119/JMST-015-0831-1
Available at: https://jmstt.ntou.edu.tw/journal/vol24/iss3/8

THE HYDRODYNAMIC CHARACTERISTICS OF AN INCLINED SUBMERGED POROUS PLATE WITH ROCK FILLED STRUCTURE

Acknowledgements

The authors wish to express their gratitude for the financial aid provided by the National Science Council, Republic of China, and Project NSC 101-2221-E-019-020.

Journal of Marine Science and Technology, Vol. 24, No. 3, pp. 434-442 (2016)
DOI: 10.6119/JMST-015-0831-1

THE HYDRODYNAMIC CHARACTERISTICS OF AN INCLINED SUBMERGED POROUS PLATE WITH ROCK FILLED STRUCTURE

Ching-Yun Yueh[1], Shih-Hsuan Chuang[2], and Chih-Hao Su[1]

Key words: inclined porous plate, permeable structure with rock filled, MBEM, reflection.

ABSTRACT

In this paper, we investigate the hydrodynamic efficiency of normal incident waves interacting with an absorbing system. The wave absorbing system consists of a submerged permeable structure filled with rock, a solid back wall, and a submerged horizontal or slightly inclined porous plate. Using a linear wave theory assumption, a multi-domain BEM (MBEM) model was created to calculate and discuss the reflection coefficients, free surface wave profiles, total wave force on the solid wall, and the horizontal and uplift forces acting on the porous plate of the water waves from several properties of the breakwater. The numerical model was calibrated using previous numerical studies to act as limiting cases for a partially submerged impermeable structure and a horizontal porous plate with a solid back wall. The accuracy of the solution is demonstrated by comparing the numerical values with those obtained from other analytical solutions. From the numerical results, the wave dissipation effect from the permeable rock-filled structure was found to perform better than expected when compared to an impermeable structure. In the case of a horizontal porous plate, the smaller submergence depth of the plate results in a smaller reflection coefficient. The larger the porous effect parameter, the smaller the value of the reflection coefficient and the larger the porous effect parameter, the greater the ability of the porous plate to reduce the uplift forces.

I. INTRODUCTION

Breakwaters are constructed to provide calm basins to protect ships from waves. The general trend in breakwater development varies from gentle slopes to vertical ones and from rubble-mound breakwaters to composites. The use of rubble mound structures or concrete caissons as wave-barriers becomes expensive as the water depth increases. Recently, many new types of breakwaters have been proposed and extensively studied to efficiently control ocean waves. In coastal engineering, there has been an emphasis on using submerged structures as breakwaters. The application of submerged horizontal plates as wave barriers can provide protection from wave attack in a semi-protected region. Previous studies show that when an incident wave encounters such a plate, a portion of the wave energy is reflected, a portion is dissipated within the vicinity of the plate, and the remainder is transmitted to the region behind the plate. The relative amounts of reflection, dissipation and transmission are dependent on the dimensions of the plate, its submergence depth, and the height and length of incident wave. This phenomenon has led to conjecture that such a plate may be used as an effective device to reduce wave forces. In recent decades, perforated breakwaters have become popular, as they allow water to pass through them, reducing the wave reflection as well as the wave run-up in front of the structure.

Several researchers have investigated the interaction of water waves using a rigid porous plate. Sollitt and Cross (1972) used Lorentz's principle of equivalent work to analyze ocean wave reflections and transmission at a permeable breakwater. Experimental measurements performed to examine reflection and transmission coefficients were carried out by Patarapanich and Cheong (1989) to validate their numerical solutions. Various studies on a single submerged horizontal porous plate for offshore wave control were reviewed by Yu (2002). Neelamani and Gayathvi (2006) experimentally investigated the performance of the dual horizontal solid plates for a wide range of wave heights and periods in regular and random waves. They found that a properly designed dual plate with a gap yields better performance than a single surface plate. Kee et al. (2007) investigated the wave blockage effect and wave energy dissipation using multi-layered submerged plates based on the linear potential theory. Liu et al. (2007) examined the hydrodynamic performance of a new perforated-wall breakwater. The breakwater consisted of a perforated front wall, a solid back wall, and a submerged horizontal porous plate installed between them. Liu et al. (2008) examined the hydrodynamic

Paper submitted 06/09/15; revised 08/05/15; accepted 08/31/15. Author for correspondence: Ching-Yun Yueh (e-mail: yuehcy@mail.ntou.edu.tw).
[1] **Department of Harbor and River Engineering, National Taiwan Ocean University Keelung, Taiwan, R.O.C.*
[2] *Wayteng Technology Co., Ltd, Kaohsiung, Taiwan, R.O.C.*

performance of a modified two-layer horizontal-plate breakwater. Numerical results show that with suitable geometrical porosity in the upper plate, the uplift wave forces on both plates can be controlled at a low level. Cho and Kim (2008) investigated the interaction of oblique incident waves with horizontal, inclined, and dual porous plates. The optimal porosity is near 0.1 and the optimal inclination angle is approximately 10° as long as the plate length is greater than 20% of the wavelength. Yueh and Chuang (2009) applied a multi-domain BEM method to calculate the reflection coefficients and the wave forces by using several absorbing-type breakwaters. Theocharis et al. (2011) experimentally studied a new type of waveabsorbing quay-wall with a single partial wave chamber containing a rock armored slope. They found that compared to a conventional solid vertical wall, the wave height in front of the wave-absorbing quay wall is reduced by 20~30%. Koraim and Rageh (2013) investigated the hydrodynamic efficiency of the vertical porous structures, wave reflection, transmission, and energy dissipation coefficients for normal and regular waves using physical models. Faraci and Liu (2014) examined the horizontal wave forces acting on combined caissons with an inner slope rubble mound based on a semi-analytical solution. The calculated results of the wave forces were validated using a multi-domain BEM solution. They found that the total horizontal wave force is insensitive to the front wall submerged depth. Altomare and Gironella (2014) provided empirical formulas for estimating reflection coefficients for low reflective quay walls with an inner slope rubble mound and two different models (large and small scale) to examine the scale effect of the inner slope rubble mound. Faraci et al. (2014) performed two laboratory campaigns focused on acquiring the reflection coefficients of the combined caissons with an adjustable front opening and chamber width that could be adjusted. The results show that the combined caissons reflection coefficients were significantly smaller than those of typical perforated caissons. Koraim et al. (2014) experimentally investigated the hydrodynamic efficiency of a new type of porous seawall using physical models. The seawall consists of a front steel screen, back solid wall, and a filled rock-core. A submerged breakwater with different parameters was installed in front of the seawall. Recently, Liu and Faraci (2014) applied step approximation theory and examined the reflection coefficients of the combined caissons by means of experimental tests and a semi-analytical solution, respectively. The results show that the optimum value can be approximately indicated as the ratio of surface-piercing rubble mound width to an incident wave length equal to 0.1.

The combined effect of a slightly inclined porous plate together with a submerged permeable structure has not been studied in detail. Thus, detailed calculations need to be carried out before designing to fully optimize the structural configuration. This paper presents the hydrodynamic characteristics of normal incident waves interacting with absorbing-type breakwaters. The absorbing-type breakwaters consist of a submerged permeable structure filled with rock, a solid back wall, and a submerged horizontal or slightly inclined porous plate. In the present study, we also discuss the effects of the porous effect parameter G, the inclined porous plate angle, and the dimensionless wave number, kh.

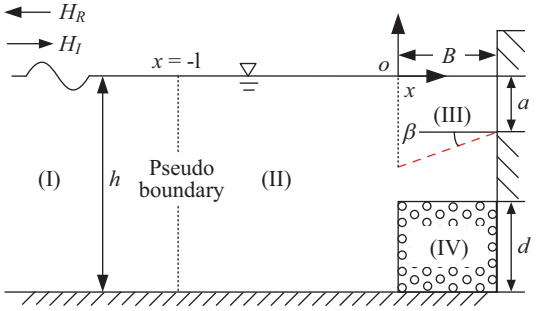

Fig. 1. Sketch of the layout.

II. THEORETICAL FORMULATION OF THE PROBLEM

A sketch of the two-dimensional problem is illustrated in Fig. 1. We consider a vertical solid back wall with the addition of a slightly inclined horizontal porous plate in a water channel of constant depth h. The angle of inclination and the submergence depth of the porous plate are denoted by β and a, respectively.

There is also a submerged, permeable rock-filled structure under the porous plate against the wall. The height and base width of the permeable structure are denoted by d and B, respectively. We denote the horizontal length of the porous plate by B, and allow the ratio of the plate thickness to water depth to be neglected. A Cartesian coordinate system ($x - y$ plane with an origin O) is taken to be the undisturbed free surface with the z-axis pointing vertically. The entire fluid domain is divided into four regions by a pseudo boundary at a distance $x = -\ell$: (I) the exterior region, (II) the intermediary region, (III) the interior region above the plate, and (IV) the interior region in the submerged permeable structure.

The usual assumption is that the fluid both outside and inside the permeable structure is inviscid, incompressible, and its motion is irrotational (Sollitt and Cross, 1972). We then define the velocity potential $\Phi^j(x, z; t)$ that satisfies the Laplace equation:

$$\nabla^2\Phi^j\left(x, z; t\right) = \frac{\partial^2\Phi^j}{\partial x^2} + \frac{\partial^2\Phi^j}{\partial z^2} = 0\,,\ \ j = I, II, III, IV\,. \quad (1)$$

The incident wave is specified to be propagating in the positive x-direction with amplitude ζ_0 and angular frequency σ. The velocity potential $\Phi^j(x, z; t)$ of the linearized wave motion may be expressed as:

$$\Phi^j\left(x, z; t\right) = \frac{g\zeta_0}{\sigma}\phi^j\left(x, z\right)\cdot\exp\left(-i\sigma t\right)\,,\ \ j = I, II, III, IV\,. \quad (2)$$

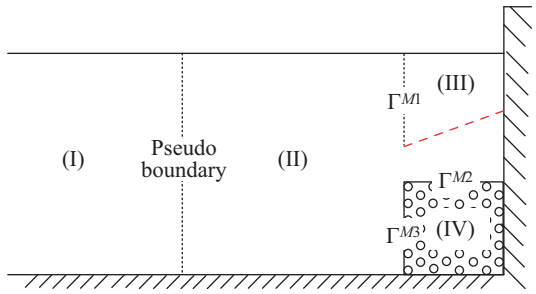

Fig. 2. Sketch of matching condition locations.

Assuming constant air pressure, the linearized boundary condition on the free surface may be obtained from the kinematic and dynamic boundary conditions:

$$\frac{\partial \phi^j}{\partial z} = \frac{\sigma^2}{g}\phi^j \text{ on } z = 0,\ j = I, II, III. \tag{3}$$

The boundary conditions on the impermeable sea bed and the surface of the fixed solid wall are given by:

$$\frac{\partial \phi^j}{\partial z} = 0 \text{ on } z = -h,\ j = I, II, IV, \tag{4}$$

$$\frac{\partial \phi^j}{\partial x} = 0 \text{ on } x = B,\ j = II, III, IV. \tag{5}$$

Fig. 2 shows the positions of the matching conditions (Γ^{M1}, Γ^{M2} and Γ^{M3}). Assuming the plate is a rigid homogeneous porous medium, the condition on the porous plate is given by:

$$\frac{\partial \phi^{\mathrm{II}}}{\partial n^{\mathrm{II}}} = -\frac{\partial \phi^{\mathrm{III}}}{\partial n^{\mathrm{III}}} = iGk\left(\phi^{\mathrm{II}} - \phi^{\mathrm{III}}\right), \tag{6}$$

where G is the porous effect parameter (Yu, 1995), n^{II} and n^{III} denote the unit outward normal vector with respect to regions (II) and (III), respectively, and k is the wave number ($= 2\pi/L$, where L is the wave length), which is defined as the real positive roots of the dispersion relation:

$$\sigma^2 = gk\tanh kh. \tag{7}$$

Because the conservation law must be satisfied over the whole computational domain and the matching condition must be imposed on Γ^{M1}, Γ^{M2} and Γ^{M3}. Thus, we obtain the following matching boundary conditions:

$$\phi^{\mathrm{II}} = \phi^{\mathrm{III}} \text{ on } \Gamma^{M1}, \tag{8}$$

$$\frac{\partial \phi^{II}}{\partial n^{II}} = -\frac{\partial \phi^{III}}{\partial n^{III}} \text{ on } \Gamma^{M1}, \tag{9}$$

$$\phi^{\mathrm{II}} = \left(S + if\right)\phi^{\mathrm{IV}} \text{ on } \Gamma^{M2} \text{ and } \Gamma^{M3}, \tag{10}$$

$$\frac{\partial \phi^{\mathrm{II}}}{\partial n^{\mathrm{II}}} = -\varepsilon\frac{\partial \phi^{\mathrm{IV}}}{\partial n^{\mathrm{IV}}} \text{ on } \Gamma^{M2} \text{ and } \Gamma^{M3}, \tag{11}$$

where ε is the porosity of the permeable structure, f is the frictional coefficient, and S is the inertia coefficient, which may be expressed using an added mass coefficient C_M (Sollitt and Cross, 1972):

$$S = 1 + \frac{1-\varepsilon}{\varepsilon}C_M. \tag{12}$$

As previously mentioned, both the mass and energy fluxes through the pseudo boundary ($x = -\ell$) must be conserved between regions (I) and (II). Thus:

$$\phi^{\mathrm{I}} = \phi^{\mathrm{II}} \text{ on } x = -\ell, \tag{13}$$

$$\frac{\partial \phi^{\mathrm{I}}}{\partial x} = \frac{\partial \phi^{\mathrm{II}}}{\partial x} \text{ on } x = -\ell. \tag{14}$$

Since the pseudo boundary at $x = -\ell$ is sufficiently far from the solid wall, so that the evanescent waves induced by the existence of a porous plate are damped enough to disappear in the region (I). The spatial velocity potential $\phi^{\mathrm{I}}(x,z)$ in the region (I) with a constant water depth h can then be expressed as follows:

$$\phi^{\mathrm{I}}(x,z) = \left[\exp\left(ik\left(x+\ell\right)\right) + R\cdot\exp\left(-ik\left(x+\ell\right)\right)\right]\frac{\cosh k\left(h+z\right)}{\cosh kh} \tag{15}$$

where R is the complex reflection coefficient.

At the pseudo boundary ($x = -\ell$), the spatial velocity potential and its normal derivative in the negative x-direction are given by

$$\phi^{\mathrm{I}} = \left(1+R\right)\frac{\cosh k\left(h+z\right)}{\cosh kh} \text{ on } x = -\ell \tag{16}$$

and

$$\frac{\partial \phi^{\mathrm{I}}}{\partial x} = ik\left(1-R\right)\frac{\cosh k\left(h+z\right)}{\cosh kh} \text{ on } x = -\ell \tag{17}$$

respectively.

By substituting Eq. (16) into Eq. (13), multiplying both sides with $\cosh k\left(h+z\right)$, and integrating from $-h$ to 0, one then has the reflection coefficient expressed as

$$R=-1+\frac{k}{N_0\sinh kh}\int_{-h}^{0}\phi^{\mathrm{II}}\cosh k\left(h+z\right)dz \quad \text{on } x=-\ell \tag{18}$$

where $N_0=\left(1+2kh/\sinh 2kh\right)/2$.

As stated before, substituting Eq. (17) into Eq. (14) yields the following equation:

$$\frac{\partial\phi^{\mathrm{II}}}{\partial x}=ik\left(1-R\right)\frac{\cosh k\left(h+z\right)}{\cosh kh} \quad \text{on } x=-\ell \tag{19}$$

The relation between ϕ^{II} and $\partial\phi^{\mathrm{II}}/\partial x$ on the pseudo-boundary is obtained

$$\frac{\partial\phi^{\mathrm{II}}}{\partial x}=\frac{2ik\cosh k\left(h+z\right)}{\cosh kh}-\frac{ik^2\cosh k\left(h+z\right)}{N_0\sinh kh\cosh kh}\int_{-h}^{0}\phi^{\mathrm{II}}\cosh k\left(h+z\right)dz \quad \text{on } x=-\ell \tag{20}$$

The hydrodynamic wave pressures P^j acting on the solid wall and the porous plate can be related to the velocity potentials through the linearized Bernoulli's equation

$$P^j=p^j\cdot\exp\left(-i\sigma t\right)=\begin{cases}-\rho\dfrac{\partial\Phi^j}{\partial t}=i\rho g\zeta_0\phi^j\cdot\exp\left(-i\sigma t\right),\ j=II,\ III\\ -\rho\left(S+if\right)\dfrac{\partial\Phi^j}{\partial t}=i\left(S+if\right)\rho g\zeta_0\phi^j\cdot\exp\left(-i\sigma t\right),\ j=IV\end{cases} \tag{21}$$

where ρ is the fluid density and the hydrostatic pressures have been neglected.

The spatial velocity potentials in region (II), (III) and (IV) satisfy the Laplace equation, using Green's second identity, they can be written as follows:

$$2\pi\phi^j\left(x,z\right)=\int_{\Gamma}\left[\phi^j\left(\xi,\eta\right)\frac{\partial\left(\ln r\right)}{\partial n}-\left(\ln r\right)\frac{\partial\phi^j\left(\xi,\eta\right)}{\partial n}\right]ds,\ j=II,\ III,\ IV \tag{22}$$

where Γ is the boundary in the region (j); $(\xi,\ \eta)$ is the coordinates of a point on the boundary Γ; $r=\sqrt{\left(x-\xi\right)^2+\left(z-\eta\right)^2}$; n is the unit outward normal vector on the boundary Γ.

We can now derive the integral representation of ϕ^j for points $P_B(\xi',\ \eta')$ lying on the boundary Γ, where the boundary is smooth. A boundary integral equation can be expressed as

$$\pi\phi^j\left(\xi',\eta'\right)=\int_{\Gamma}\left[\phi^j\left(\xi,\eta\right)\frac{\partial\left(\ln r'\right)}{\partial n}-\left(\ln r'\right)\frac{\partial\phi^j\left(\xi,\eta\right)}{\partial n}\right]ds,\ j=II,\ III,\ IV \tag{23}$$

where $r'=\sqrt{\left(\xi'-\xi\right)^2+\left(\eta'-\eta\right)^2}$.

The boundary Γ in Eq. (23) is discretized into N^j constant elements, where N^j is the number of constant elements in the region (j). The values of the boundary quantity ϕ^j and its normal derivative $\partial\phi^j/\partial n$ are assumed constant over each element and equal to their value at the mid-point of the element. In the numerical analysis, the discretized form of Eq. (23) can be applied consecutively for all the nodes yielding a system of N^j linear algebraic equations, which can be re-written in a matrix form as follows:

$$\left[\bar{U}^j\right]\left\{\phi^j\right\}=\left[U^j\right]\left\{\frac{\partial\phi^j}{\partial n}\right\},\ j=II,\ III,\ IV \tag{24}$$

Where

$$\bar{U}^j_{\alpha\lambda}=\int_{\Gamma_\lambda}\frac{\partial\left(\ln r'\right)}{\partial n}ds_\lambda-\pi\delta_{\alpha\lambda},\ j=II,\ III,\ IV \tag{25}$$

$$U^j_{\alpha\lambda}=\int_{\Gamma_\lambda}\left(\ln r'\right)ds_\lambda,\ j=II,\ III,\ IV \tag{26}$$

in which $\delta_{\alpha\lambda}$ is the Kronecker delta, which is equal to 1 when $\alpha=\lambda$ and 0 otherwise.

For the numerical computations, using the boundary element technique, Eq. (24) can be written in another matrix form:

$$\begin{bmatrix}\left[\bar{U}^{\mathrm{II}}\right]&0&0\\0&\left[\bar{U}^{\mathrm{III}}\right]&0\\0&0&\left[\bar{U}^{\mathrm{IV}}\right]\end{bmatrix}\begin{Bmatrix}\left\{\phi^{\mathrm{II}}\right\}\\\left\{\phi^{\mathrm{III}}\right\}\\\left\{\phi^{\mathrm{IV}}\right\}\end{Bmatrix}=\begin{bmatrix}\left[U^{\mathrm{II}}\right]&0&0\\0&\left[U^{\mathrm{III}}\right]&0\\0&0&\left[U^{\mathrm{IV}}\right]\end{bmatrix}\begin{Bmatrix}\left\{\dfrac{\partial\phi^{\mathrm{II}}}{\partial n}\right\}\\\left\{\dfrac{\partial\phi^{\mathrm{III}}}{\partial n}\right\}\\\left\{\dfrac{\partial\phi^{\mathrm{IV}}}{\partial n}\right\}\end{Bmatrix} \tag{27}$$

By substituting the boundary conditions, Eqs. (3)-(6), Eqs. (8)-(11) and Eq. (20) into Eq. (27), the linearized solutions of the spatial velocity potential on each boundary can be obtained. The reflection coefficient on the pseudo boundary can be evaluated from Eq. (18). Then the hydrodynamic force exerted on the solid wall and the surface of the porous plate per unit width can be determined by integrating the pressure distributions (Eq. (21)), respectively. Hence

$$F_w=\int_{-h}^{0}P^j dz=i\rho g\zeta_0\left[\left(S+if\right)\int_{-h}^{-h+d}\phi^{\mathrm{IV}}dz+\int_{-h+d}^{-a}\phi^{\mathrm{II}}dz+\int_{-a}^{0}\phi^{\mathrm{III}}dz\right]\cdot\exp\left(-i\sigma t\right) \quad \text{on } x=B \tag{28}$$

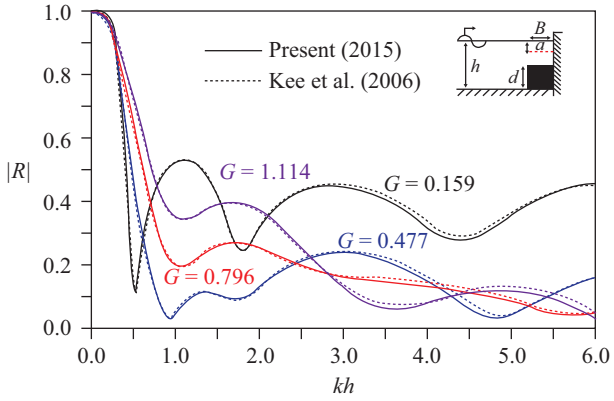

Fig. 3. Variation in $|R|$ versus kh for various values of G ($\beta = 0°$, $B/h = 1.0$, $a/h = 0.1$, and $d/h = 0.5$).

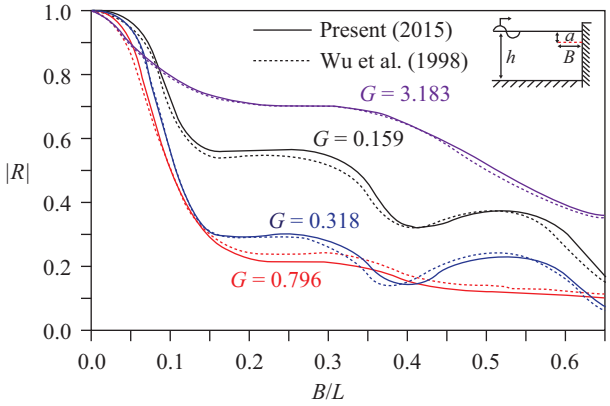

Fig. 4. Variation in $|R|$ versus dimensionless relative plate length B/L ($\beta = 0°$, $a/h = 0.2$, and $kh = 1.571$).

$$F_{ph} = \int P^j dB_p \cdot (-\sin\beta) = -i\rho g\zeta_0 \left[\int \left(\phi^{II} - \phi^{III}\right) dB_p\right] \cdot \exp(-i\sigma t)\sin\beta \quad \text{on the porous plate} \tag{29}$$

$$F_{pv} = \int P^j dB_p \cdot \cos\beta = i\rho g\zeta_0 \left[\int \left(\phi^{II} - \phi^{III}\right) dB_p\right] \cdot \exp(-i\sigma t)\cos\beta \quad \text{on the porous plate} \tag{30}$$

where F_w denotes the total wave force per unit width on the solid wall; F_{ph} and F_{pv} represent the total horizontal and uplift force per unit width acting on the porous plate, respectively; with B_p, the length of the porous plate.

III. VERIFICATION OF THE NUMERICAL METHOD

The multi-domain boundary element method (MBEM), as described in section 2, is applied to study the hydrodynamic characteristics of an inclined submerged porous plate with rock filled structure. To examine the reliability and accuracy of the numerical method, three cases are presented and discussed in this section. The accuracy of the solution is demonstrated by comparing the numerical values with those obtained from other analytical solutions. In the first example, the present breakwater becomes a caisson breakwater with an internal horizontal porous plate, and the submerged permeable structural segment becomes a rectangular submerged impermeable structure ($\varepsilon = 0$). A comparison of the reflection coefficient $|R|$ in this case with that from this model and the results from Kee et al. (2006) are shown in Fig. 3. The dashed lines represent Kee's (2006) solution, and we see that the present results (solid lines) agree fairly well. As the porosity parameters increase, the reflection coefficient gradually decreases to a certain porosity parameter $G = 0.477$ for a relatively wide range of kh. For relatively larger porosity parameters, such as $G = 0.796$ and 1.114, the reflected waves gradually increase.

In the second case, which is shown in Fig. 4, the ratio of the submerged permeable structure height to the water depth is taken to be $d/h = 0$, resulting in a vertical wall with a horizontal submerged porous plate. These plots are compared to solutions (dashed lines) from Wu et al. (1998), using the eigenfunction expansion method. The larger the porous plate, the smaller the reflection coefficient; this is because the loss of incident wave energy is directly proportional to the length of the porous plate.

Finally, the absolute value of the dimensionless wave amplitude (η) normalized by the incident wave amplitude (a) is depicted in Fig. 5 and Fig. 6. The x-axis is the calculate region, wave propagating from X/h = -4.5 to X/h = 3.5, dividing into 320 elements. The y-axis is the non-dimensioal wavenumber (kh), kh = 0.01 to 4.01 interval 0.025. The red continuous line and dashed line indicate the impermeable plate and porous plate, respectively. A standing wave is formed in the front of the submerged impermeable plate located at -1.0 ≤ Xh ≤ 0.0. Fig. 5 shows the dimensionless wave amplitude profiles versus kh and x/h for an impermeable plate with $G = 0.0$, $B/h = 1.0$, and $a/h = 0.1$. Fig. 5 (a) shows the results from Kee et al. (2007), and Fig. 5 (b) shows our numerical results. The standing wave is further intensified, especially in the narrow high frequency regions. Fig. 6 shows the dimensionless wave amplitude profiles versus kh and X/h for a prous plate with $G = 0.796$, $B/h = 1.0$, and $a/h = 0.1$. Fig. 6 shows the wave energy dissipation effects that suppress the reflected and transmitted waves simultaneously. It is interesting to note that the dimensionless wave amplitude noticeably decreases over the submerged porous plate, particularly for higher frequency ranges (Kee et al., 2007).

From the above comparisons, we conclude that the method proposed here is appropriate and reliable for analyzing the hydrodynamic characteristics of an inclined submerged porous plate with rock filled structure.

In the following numerical examples, we adopt the geometric parameters $B/h = 1.0$, $a/h = 0.1$, and $d/h = 0.5$ and the permeability parameters $S = 1.0$ and $\varepsilon = 0.6$. In the original

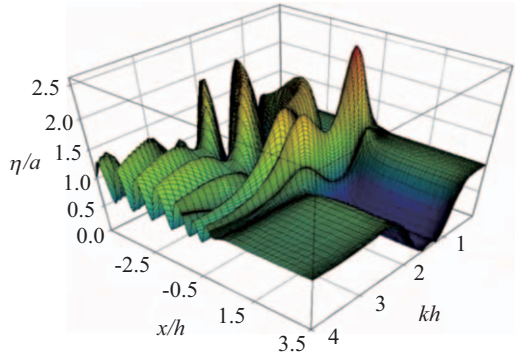

(a) Kee et al. (2007)

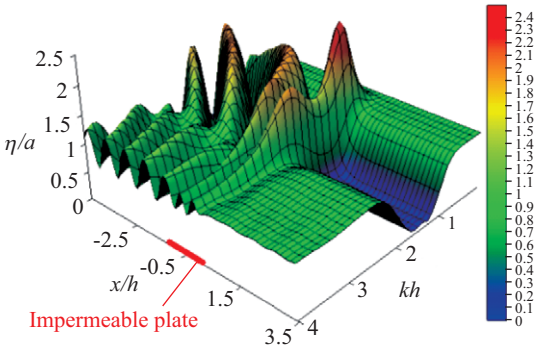

(b) Present results (2015)

Fig. 5. Dimensionless wave amplitude profiles versus *kh* and *x*/*h* (G = 0.0, *B*/*h* = 1.0, *a*/*h* = 0.1, and -1.0 ≤ *X*/*h* ≤ 0.0).

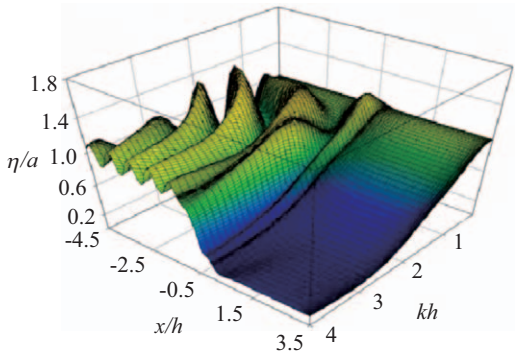

(a) Kee et al. (2007)

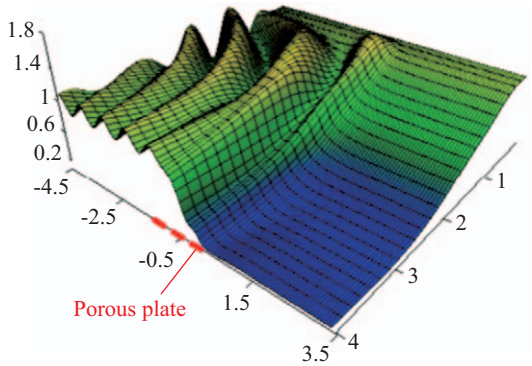

(b) Present results (2015)

Fig. 6. Dimensionless wave amplitude profiles versus *kh* and *x*/*h* (G = 0.796, *B*/*h* = 1.0, *a*/*h* = 0.1, and -1.0 ≤ *X*/*h* ≤ 0.0).

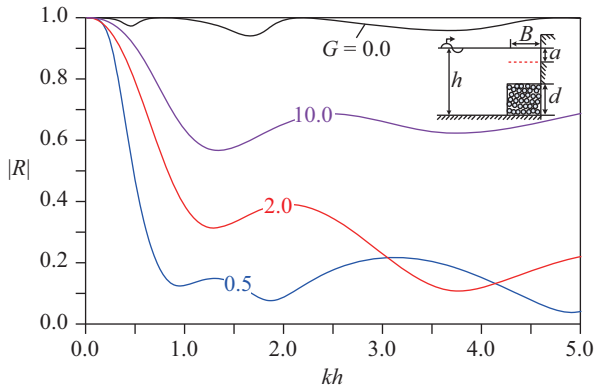

Fig. 7. Reflection coefficient |*R*| as a function of kh and *G* (*β* = 0°, *B*/*h* = 1.0, *a*/*h* = 0.1, and *d*/*h* = 0.5).

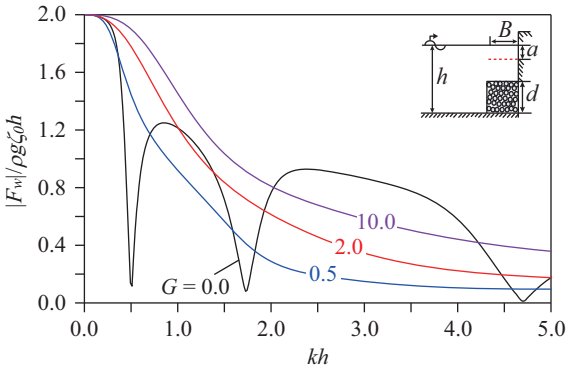

Fig. 8. Dimensionless solid wall wave force $|F_w|/\rho g\zeta_0 h$ as a function of *kh* and *G* (*β* = 0°, *B*/*h* = 1.0, *a*/*h* = 0.1, and *d*/*h* = 0.5).

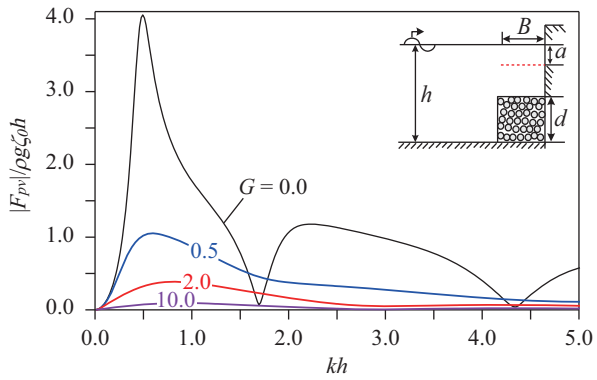

Fig. 9. Dimensionless porous plate uplift force $|F_{pv}|/\rho g\zeta_0 h$ as a function of *kh* and *G* (*β* = 0°, *B*/*h* = 1.0, *a*/*h* = 0.1, and *d*/*h* = 0.5).

formulation of Sollitt and Cross (1972), the frictional coefficient (f) is calculated implicitly using the Lorentz principle of equivalent work. In the present paper, the frictional coefficient (f) is treated simply as a constant f = 1.8 that is assumed to be known.

The resulting wave reflection coefficients, the total wave force exerted on the wall, the horizontal and uplift forces acting on the porous plate, and the free-surface wave profiles are shown in Figs. 7-13.

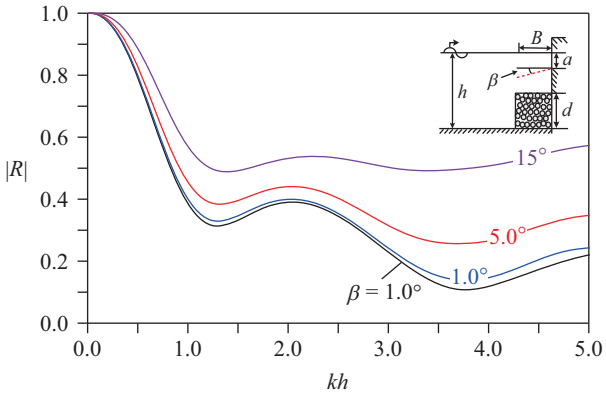

Fig. 10. Reflection coefficient $|R|$ as a function of kh and β (G = 2.0, B/h = 1.0, a/h = 0.1, and d/h = 0.5).

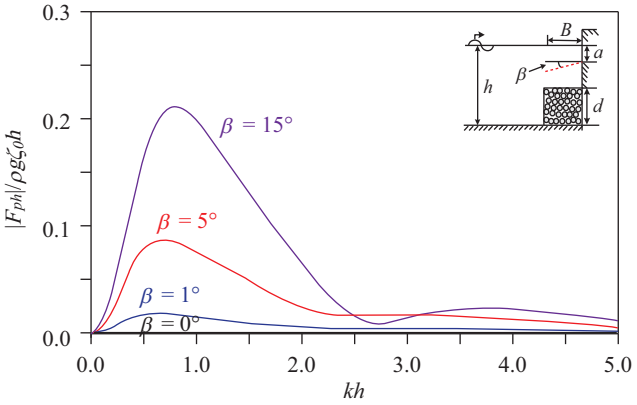

(a) Dimensionless horizontal force

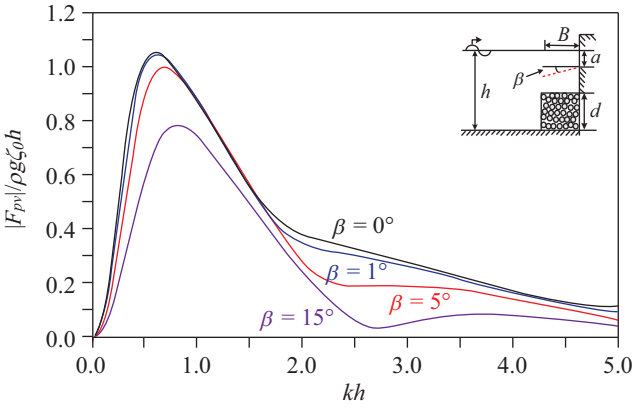

(b) Dimensionless uplift force

Fig. 11. Dimensionless porous plate horizontal and uplift forces as a function of kh and β (G = 0.5, B/h = 1.0, a/h = 0.1, and d/h = 0.5).

IV. RESULTS AND DISCUSSION

1. Porous Effect Parameter (G)

The porous effect parameter G is one of the most important parameters related to wave reflection from the present breakwater discussed in this paper. In our numerical model, the value of the energy dissipation coefficient E_L used to es-

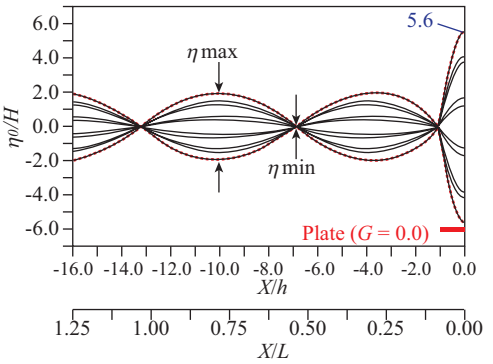

(a) kh = 0.4933, L/h = 12.737 and $|F_{pv}|_{max}$ = 4.054

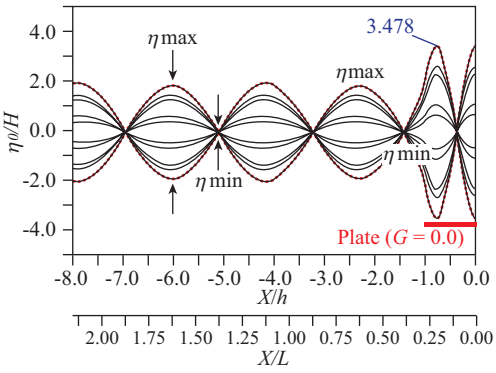

(b) kh = 1.693, L/h = 3.711 and $|F_{pv}|_{min}$ = 0.069

Fig. 12. The free surface profiles above the submerged impermeable plate at (a) kh = 0.4933 and (b) kh = 1.693 (G = 0.0).

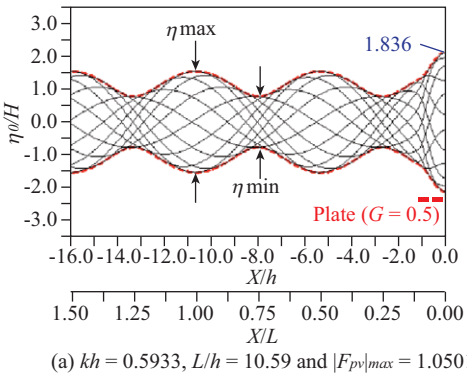

(a) kh = 0.5933, L/h = 10.59 and $|F_{pv}|_{max}$ = 1.0501

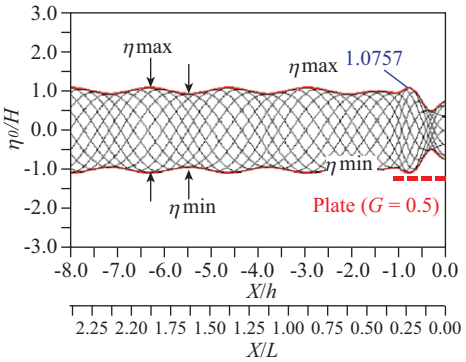

(b) kh = 1.8767, L/h = 3.348 and $|F_{pv}|_{min}$ = 0.3982

Fig. 13. The free surface profiles above the submerged porous plate at (a) kh = 0.5933 and (b) kh = 1.8767 (G = 0.5).

timate the wave energy dissipation at the complex breakwater is a function of $|R|$. From a conservation of energy perspective, $|R|$ is related to the energy dissipation coefficient $E_L = 1 - |R|^2$.

Fig. 7 shows the reflection coefficient $|R|$ as a function of kh for different values of G, where the angle of inclination of the submerged porous plate is $\beta = 0°$. This figure indicates that as the dimensionless wave number kh increases from 0.0 to 1.0, the reflection coefficients $|R|$ dramatically decrease as a result of the wave energy dissipation through fine pores on the plate for each non-zero value of G (excluding the impermeable plate $G = 0$). Then, the variation in $|R|$ decreases over the range kh = 1.0~5.0. As $kh \to 0$, the wavelength L of the incident wave is very long with respect to the water depth h. Thus, the wave does not feel the porous plate and the submerged permeable structure, and the corresponding total reflection ($|R| = 1.0$) from the impermeable solid back wall is noticeable.

The dimensionless wave force per unit width of the solid wall and the dimensionless porous plate uplift force as functions of kh are shown in Fig. 8 and Fig. 9, respectively, for the same conditions. As the value of kh increases, the value of $|F_w|/\rho g\zeta_0 h$ decreases (with the exception of the impermeable plate case ($G = 0$). The value of $|F_w|/\rho g\zeta_0 h$ may be calculated by integrating the pressure over the depth per unit width of the wall if only a vertical solid wall is used in the water channel. Hence, the maximum dimensionless wave force is: $|F_w|/\rho g\zeta_0 h = 2\tanh kh/kh$ (Dean and Dalrymple, 1991).

As mentioned, the wave does not feel these structures, except for the solid back wall as $kh \to 0$. In other words, the value of $|F_w|/\rho g\zeta_0 h$ can be obtained as $kh \to 0$, and therefore decreases from 2.0, as shown in Fig. 8.

In Fig. 9, a strong decrease in the value of $|F_{pv}|/\rho g\zeta_0 h$ appears from the impermeable plate case ($G = 0$) to the porous plate cases, indicating that the value of $|F_{pv}|/\rho g\zeta_0 h$ decreases as G increases. The peak of $|F_{pv}|/\rho g\zeta_0 h$ ($|F_{pv}|_{\max}$) approaches 4.054 when kh = 0.4933, and the minimum wave force for the impermeable case $G = 0$ is $|F_{pv}|_{\min} \approx 0.069$, which occurs at kh = 1.693. Fig. 9 shows that as the porous effect parameter G increases, the value of the uplift force decreases. This loss of incident wave energy is directly proportional to the porous effect parameter (G). Here, the dimensionless uplift force monotonically decreases as the porous effect parameter increases.

2. Inclined Angle (β)

Fig. 10 depicts the relationship between $|R|$ and kh for different values of the inclined angle β. In this example, the porous effect parameter G = 2.0 is used. The main characteristic of $|R|$ as a function of kh in Fig. 10 is similar to that observed in Fig. 7. The reflection coefficient $|R|$ increases with the inclined angle β.

Repeating this procedure and using G = 0.5, the dimensionless porous plate horizontal and uplift forces as functions of kh are shown in Fig. 11. The influence of β on the plate horizontal and vertical force is positive, hence the value of $|F_{ph}|/\rho g\zeta_0 h$ increases and the value of $|F_{pv}|/\rho g\zeta_0 h$ decreases as the value of β increases. Therefore, the value of $|F_{pv}|/\rho g\zeta_0 h$ is much larger than the value of $|F_{ph}|/\rho g\zeta_0 h$ in this example.

3. The Dimensionless Free Surface Wave Profiles (η_0/H)

The dimensionless free surface profiles ahead of the wall are presented in Figs. 12 and 13 for G = 0.0 and G = 0.5, respectively, for several different kh values, describing the maximum and minimum uplift force acting on the impermeable and porous plate. We note from these results that the waves may focus in the region close to the solid wall. For an impermeable plate (G = 0.0), there exists a significant wave focusing process. We note that in the vicinity of the solid back wall, the relative wave height is greater than 2.0. For a partial standing wave field, quasi-nodes and quasi-antinodes alternate spatially at X-locations in increments of $L/4$. This is seen in Figs. 12 (a) and (b). Quasi-nodes occur at X/L = 0.25 and 0.75 and quasi-antinodes occur at X/L = 0.5 and 1.0. In Fig. 12(a), examining the free surface profiles above the submerged impermeable plate shows that there is a node located at the left end of the plate, resulting in a maximum uplift force. However, in Fig. 12 (b), there is a node located in the middle and above the plate, resulting in a minimum uplift force.

For a porous plate, as G increases from zero to G = 0.5, the effect of the permeability tends to weaken the wave focusing process (Wu et al., 1998). For a porous plate, if the porous effect parameter G is small and the relative plate length (B/L) is fixed, the relative wave height on the solid back wall will be less than 2.0. These results reveal that there are remarkable differences between the wave focusing over a plate, which occurs in the vicinity of the wall for an impermeable plate and a porous plate. For a porous plate, the increase in the porous effect parameter leads to dissipation of the incident wave energy and tends to weaken the wave focusing process.

V. CONCLUSIONS

In this paper, the hydrodynamic efficiency of normal incident waves interacting with a submerged slightly inclined porous plate wave absorber was investigated using a multi-domain BEM (MBEM). The linear wave theory was adopted in this model. The accuracy and validity of the method was verified through numerical comparisons of the reflection coefficients and dimensionless free surface wave profiles from results obtained by other authors using different methods.

The salient conclusions drawn from this paper are as follows. In the proposed structure, the larger the porous effect

parameter, the smaller the value of the reflection coefficient and the larger the porous effect parameter, the greater the ability of the porous plate to reduce the uplift forces. It is also demonstrated that the uplift wave forces acting on a porous plate are smaller than those acting on an impermeable plate. The inclined angle of the plate changes the geometric shape of the present breakwater and affects the reflection, horizontal and vertical wave forces on the plate. As the inclined angle increases, both the reflection coefficient and the value of horizontal force increases but the value of vertical force decreases. The increase in the porous effect parameter leads to dissipation of the incident wave energy and tends to weaken the wave focusing process. From the free surface profiles above the submerged impermeable plate shows that if there is a node located at the left end of the plate, resulting in a maximum uplift force. However, if there is a node located in the middle and above the plate, resulting in a minimum uplift force. It is worth noting that the MBEM model may be applied to more general complex structural systems by assigning a realistic porous effect parameter.

ACKNOWLEDGMENTS

The authors wish to express their gratitude for the financial aid provided by the National Science Council, Republic of China, and Project NSC 101-2221-E-019-020.

REFERENCES

Altomare, C. and X. Gironella (2014). An experimental study on scale effects in wave reflection of low-reflective quay walls with internal rubble mound for regular and random waves. Coastal Engineering 90, 51-63.

Cho, H. and M. H. Kim (2008). Wave absorbing system using inclined perforated plates. Journal of Fluid Mechanics 608, 1-20.

Faraci, C. and Y. Liu (2014). Analysis of wave forces acting on combined caissons with inner slope rubble mound. Coastal Engineering 34.

Faraci, C., P. Scandura and E. Foti (2014). Reflection of sea waves by combined caissons. Journal of Waterway, Port, Coastal and Ocean Engineering, DOI: 10.1061/(ASCE)WW.1943-5460.0000275.

Kee, S. T., S. H. Lee and J. S. Ko (2006). Submerged porous plate wave absorber. proceedings of the sixteen (2006) Int. Offshore and Polar Eng. Conf, San Francisco, USA, ISOPE 3, 626-631.

Kee, S. T, S. H. Lee and J. S. Ko (2007). Blockage effects and wave energy dissipation by submerged porous plates. International Offshore and Polar Engineering Conference, ISOPE 17, 2546-2553.

Koraim, A. S. and O. S. Rageh (2013). Hydrodynamic performance of vertical porous structures under regular waves. China Ocean Engineering 27, 4, 451-468.

Koraim, A. S., E. M. Heikal and A .A. Abo Zaid (2014). Hydrodynamic characteristics of porous seawall protected by submerged breakwater. Applied Ocean Research 46, 1-14.

Liu, Y., Y. C. Li and B. Teng (2007). Wave interaction with a perforated wall breakwater with a submerged horizontal porous plate. Ocean Engineering 34, 17-18.

Liu, Y., Y. C. Li and B. Teng (2008). Wave motion over a submerged breakwater with an upper horizontal porous plate and a lower horizontal solid plate. Ocean Engineering 35, 1588-1596.

Liu, Y. and C. Faraci, (2014). Analysis of orthogonal wave reflection by a caisson with open front chamber filled with sloping rubble mound Coastal Engineering 91, 151-163

Neelamani, S. and T. Gayathri (2006). Wave Interaction with twin plate wave barrier. Ocean Engineering 33, 495-516.

Patarapanich, M. and H. F. Cheong (1989). Reflection and transmission characteristics of regular and random waves from a submerged horizontal plate. Coastal Engineering 13(2), 161-182.

Sollitt, C. K. and R. H. Cross (1972). Wave transmission through permeable breakwaters. Proc. 13th Coastal Eng. Conf., New York, ASCE 3, 1827-1846.

Theocharis, I., E. N. Anastasaki, C. I. Moutzouris and T. Giantsi (2011). A new wave absorbing quay-wall for wave height reduction in a harbor basin. Ocean Engineering 38, 1967-1978.

Wu, J., Z. Wan and F. Fang (1998). Wave reflection by a vertical wall with a horizontal submerged porous plate. Ocean Engineering 25(9), 767-779.

Yueh, C. Y. and S. H. Chuang (2009). Wave scattering by a submerged porous plate wave absorber. The International Society of Offshore and Polar Engineers 1167-1173.

Yu, X. (1995). Diffraction of water waves by porous breakwaters. Journal of Waterway, Port, Coastal, and Ocean Engineering, ASCE 121, 275-282.

Yu, X. (2002). Functional performance of a submerged and essentially horizontal plate for offshore wave control: a review. Coastal Engineering Journal 44(2), 127-147.